






RESEARCH ARTICLE | AUGUST 22 2024


Raman enhancement via double optical resonances in all-dielectric photonic crystal slabs


Yuyang Xu; Shunben Wu; Shaoxin Hong; Xinhao Wang; Xiaohan Liu; Jiajun Wang ; Lei Shi *Appl. Phys. Lett.* 125, 081704 (2024)<https://doi.org/10.1063/5.0226837>

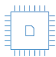
 Nanotechnology & Materials Science

 Optics & Photonics

 Impedance Analysis

 Scanning Probe Microscopy

 Sensors

 Failure Analysis & Semiconductors



Unlock the Full Spectrum.
From DC to 8.5 GHz.

Your Application. Measured.

[Find out more](#)



Raman enhancement via double optical resonances in all-dielectric photonic crystal slabs

Cite as: Appl. Phys. Lett. **125**, 081704 (2024); doi: [10.1063/5.0226837](https://doi.org/10.1063/5.0226837)

Submitted: 4 July 2024 · Accepted: 10 August 2024 ·

Published Online: 22 August 2024



View Online



Export Citation



CrossMark

Yuyang Xu,¹ Shunben Wu,¹ Shaoxin Hong,¹ Xinhao Wang,¹ Xiaohan Liu,^{1,2} Jiajun Wang,^{1,a)} and Lei Shi^{1,2,3,4,a)} 

AFFILIATIONS

¹State Key Laboratory of Surface Physics, Key Laboratory of Micro- and Nano-Photonic Structures (Ministry of Education) and Department of Physics, Fudan University, 200433 Shanghai, China

²Institute for Nanoelectronic Devices and Quantum Computing, Fudan University, 200438 Shanghai, China

³Collaborative Innovation Center of Advanced Microstructures, Nanjing University, Nanjing, 210093 Jiangsu, China

⁴Shanghai Research Center for Quantum Sciences, 201315 Shanghai, China

^{a)}Authors to whom correspondence should be addressed: jiajunwang@fudan.edu.cn and lshi@fudan.edu.cn

ABSTRACT

All-dielectric photonic structures are an important class of substrates in surface-enhanced Raman spectroscopy (SERS), utilizing optical resonant modes to significantly enhance the electromagnetic field and amplify the Raman signals. In this study, we demonstrate the double-resonance approach to realize significant Raman enhancement using all-dielectric photonic crystal (PhC) slab. The double-resonance condition is satisfied by designing optical resonant modes in photonic bands to match frequencies of both excitation laser and Raman signals. By the fabricated PhC slab, the significant enhancement for the Raman signal of silicon is demonstrated. The enhanced Raman signals exhibit a uniform distribution on the PhC slab. The method of Raman enhancement via double optical resonances can advance the field of all-dielectric SERS and holds potential for future SERS applications.

Published under an exclusive license by AIP Publishing. <https://doi.org/10.1063/5.0226837>

Raman spectroscopy is a powerful tool for real-time and nondestructive analysis of material composition due to the ability to identify the unique spectral fingerprint of vibrations.^{1–4} Widely employed in fields like chemistry,^{5,6} biology,^{7–9} and medical diagnostics,^{10,11} Raman spectroscopy still suffers from the inherently weak intensity of Raman scattering light.^{2,12} This limitation impedes its application, particularly in situations requiring high sensitivity. Consequently, the enhancement of Raman signals remains a critical objective in the field of Raman spectroscopy.

Surface-enhanced Raman spectroscopy (SERS) is currently the most common scheme for Raman enhancement. Typically, SERS is bifurcated into two categories according to the substrate materials used: metal-based SERS and all-dielectric SERS.^{13–15} In metal-based SERS, the electromagnetic mechanism (EM) serves as the primary driver for Raman enhancement.^{13,16} For electromagnetic field enhancement, noble metals, such as Au and Ag, are used in the substrate to create localized hotspots via surface plasmon resonances. When the sample is located on the sharp hotspots, the Raman signal from the sample can be significantly amplified, achieving a super-high enhancement factor.^{2,15,17}

Beyond metal-based SERS, there has also been considerable interest and extensive research into all-dielectric SERS in recent years. This

approach not only reduces material costs but also introduces a series of properties. In the past period of time, all-dielectric SERS substrates primarily relied on the chemical mechanism (CM) like charge transfer as the main mechanism for achieving Raman enhancement. The performance of Raman enhancement through CM has been extensively studied with a wide variety of nonmetallic substrates, especially two-dimensional (2D) material substrates.^{18–20}

In addition to CM, achieving stronger electromagnetic field enhancement is also expected in all-dielectric SERS. For the application of EM in all-dielectric SERS, resonant modes are required for the non-metallic substrate.^{14,21–23} In the field of nano-photonics, the resonant modes can be constructed by the structural design, using all-dielectric materials.^{24–26} Among various nanophotonic structures, photonic crystal (PhC) slabs, featuring various optical resonant modes,^{27,28} have emerged as a powerful platform for Raman enhancement through EM. Constructed from periodic dielectric structures, PhC slabs can have photonic bands due to the Bloch scattering. Considering optical modes in the photonic band, which are above the light line (resonant modes), they can couple with propagating waves in free space with the same in-plane momentum. When light shines on the PhC slab and couples with these resonant modes, optical resonances can lead to near-field electromagnetic field enhancement, leading to enhancement

applications in infrared absorption,²⁹ nonlinear generation,³⁰ etc. Leveraging a similar optical resonance mechanism, Raman enhancement has been initially explored in various dielectric structures. The previous studies predominantly focused on the enhancement at the excitation laser frequency [denoted as ω in Fig. 1(a)]. When the excitation laser is enhanced in the near-field region, a corresponding enhancement in the Raman signal [with frequency ω' , as denoted in Fig. 1(a)] can be observed.^{31–33} In addition, the Raman signal can be also directly amplified through the field enhancement supported by resonance at ω' frequency. Then, if the optical resonances are concurrently available at the frequency of both ω and ω' (double resonances), it is expected to achieve a better enhancement factor. However, to date, there are rare reports of Raman enhancement by utilizing double optical resonances.

Here, we demonstrate a PhC slab with double-resonance design for Raman enhancement. To match the double-resonance condition, the photonic bands of the PhC slab are designed to overlap with both the excitation laser frequency (ω) and Raman signal frequency (ω'). By the fabricated PhC slab, the Raman enhancement induced by double optical resonances for the first-order Raman peak of silicon is demonstrated. This enhancement exhibits a uniform spatial distribution due to the periodicity of the PhC slab. Comparatively, the Raman enhancement induced by the double-resonance approach achieves a higher enhancement factor than the single-resonance cases.

Figure 1(a) shows the schematic view of Raman scattering in a PhC slab made of silicon. In this case, the Raman signals of silicon are applied to exhibit our proposed method of Raman enhancement via double optical resonances. We employ a laser with a wavelength of 785 nm as the excitation light, corresponding to the frequency of ω in

Fig. 1(a). Upon incidence of this laser, the Raman scattering light from silicon's first-order optical phonon will be emitted with a wavelength of 818.4 nm, corresponding to the frequency of ω' in Fig. 1(a). The frequency difference between the scattered light and incident light, 520.7 cm^{-1} , corresponds to the vibration frequency of the first-order optical phonon. This signal is the typical first-order Raman peak for silicon.

To start, we designed a PhC slab to match the double-resonance condition of the mentioned experimental setup. The PhC slab is fabricated by a 100-nm monocrystalline silicon film on the sapphire substrate. It has a two-dimensional periodic square lattice structure, with period $a = 340 \text{ nm}$. Within each unit cell, a cylindrical hole is etched on the silicon layer with diameter $d = 190 \text{ nm}$. The simulated photonic bands of this PhC slab are depicted by black lines in Fig. 1(b). The photonic bands of the PhC slab are simulated using the finite element method. The orange and red lines in Fig. 1(b) represent the wavelength of the excitation laser (ω) and the first-order Raman peak (ω'). Both lines intersect with the photonic band of PhC slab, meaning the double-resonance condition is matched. In Fig. 1(c), we exhibit the electric field distributions in a cross section of the structure (outlined by dashed lines), corresponding to the dot-marked resonant modes in Fig. 1(b). For both modes, the fields are confined and overlapped in the etched silicon layer. Based on the designed resonant-induced field enhancement for frequencies of both excitation light and Raman signal, we can expect the double-resonance-induced Raman enhancement.

To experimentally characterize the Raman enhancement effect, we fabricated the designed PhC slab. Figure 2(a) shows the scanning electron micrograph of the sample. Then, we measured the angle-resolved transmittance spectra using a homemade momentum-space imaging spectroscopy based on the Fourier optics^{34,35} (see the experimental setup in the supplementary material, Fig. S1). The results are shown in Fig. 2(b). The dispersion of the sample is exhibited clearly in the spectra. The results agree well with the simulated photonic bands in Fig. 1(b). The red solid line and dashed line represent the frequencies of excitation laser (ω) and the first-order Raman peak (ω'), respectively. We can see both lines overlap with the photonic bands of the PhC slab, meaning that the condition of double resonance is satisfied in this sample.

Next, we measured the Raman spectra of the sample (see the experimental setup in the supplementary material, Fig. S2). The result is shown in Fig. 2(c). The orange and blue lines present the Raman spectra of the PhC slab and the unstructured flat silicon film. The first-order Raman peak is marked by the red dashed line. It is significantly enhanced in the Raman spectrum of the PhC slab, comparing with the spectrum of flat silicon film. To identify and exclude the influence of substrate, we also measured the Raman spectrum of a bare sapphire substrate, as depicted by the black line. It presents typical Raman peaks of sapphire, and all of these peaks do not overlap with silicon's first-order Raman peak. Then, we calculated the enhancement factor (EF) of the PhC slab by $\text{EF} = I_{\text{PhC}}/I_{\text{Si}}$, where I_{PhC} is the intensity of the Raman spectrum of the PhC slab and I_{Si} represents the intensity of the Raman spectrum of the flat silicon film. The results are shown in Fig. 2(d). Under the double-resonance condition, the PhC slab provides a maximum enhancement up to 180 times for the Raman signal. The effective enhancement area can be also taken into account when calculating the enhancement factor.³⁶ Due to the etched holes in the PhC slab, the amount of silicon participating in the Raman scattering

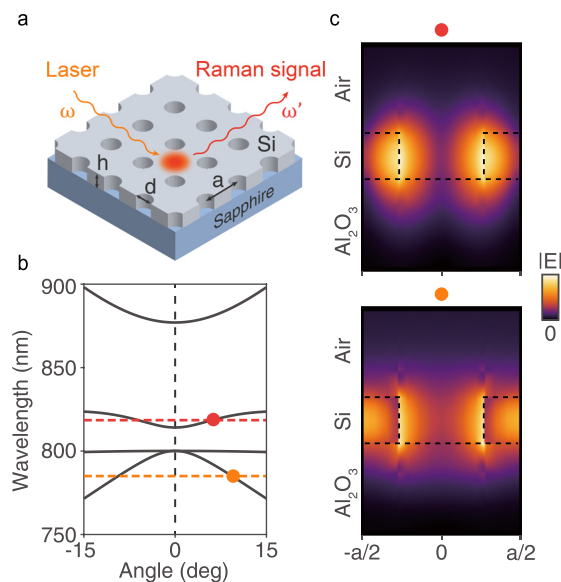


FIG. 1. (a) Schematic view of Raman scattering in a PhC slab. (b) Simulated photonic bands of the PhC slab. The wavelengths of excitation laser and silicon's first-order Raman peak are marked by orange and red dashed lines. (c) Simulated electric field distribution of the modes marked by dots in (b). The dashed lines outline the interface between air, silicon, and the Al_2O_3 substrate. The width plotted corresponds to the period of the PhC slab.

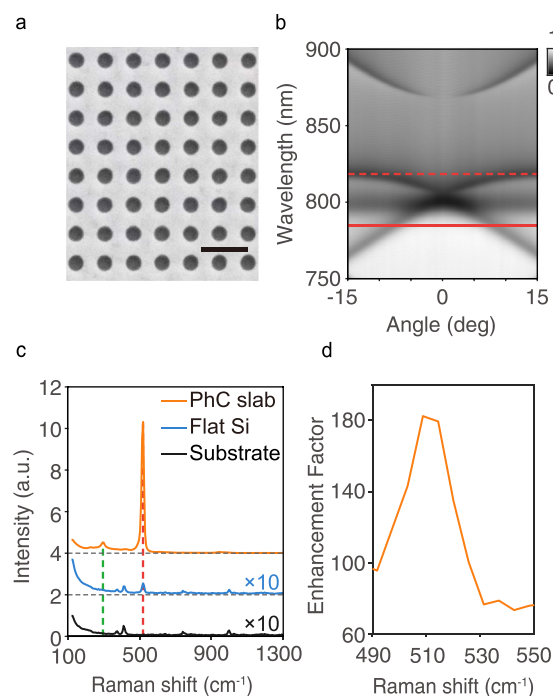


FIG. 2. (a) Scanning electron micrograph of the PhC slab sample (scale bar, 500 nm). (b) Measured angle-resolved transmittance spectrum of the PhC slab. The wavelengths of laser and first-order Raman peak of silicon are marked by solid line and dashed line, respectively. (c) Measured Raman spectra. Black line: Raman spectrum of sapphire substrate, scaled by 10 times; blue line: Raman spectrum of flat silicon film, scaled by 10 times, intensity offset: +2; and orange line: Raman spectrum of the PhC slab, intensity offset: +4. Red dashed line: first-order Raman peak; and green dashed line: the signal from second-order Raman scattering. (d) Enhancement factor of the PhC slab.

process is less, compared to the case of the flat silicon film. When considering the area ratio occupied by silicon (about 75%), the maximum enhancement factor provided by the PhC is 240. The enhancement factors vary for different frequencies, and it causes a slight deviation in the line shape of silicon's first-order Raman peak (see details in the [supplementary material](#), Fig. S3). We also measured the Raman spectra of the PhC slab under different power of excitation laser. The results are shown in the [supplementary material](#), Fig. S4. The intensity of enhanced first-order Raman peak is proportional to the laser power, which is commonly seen in the spontaneous Raman scattering.

In addition to the first-order Raman peak, a signal from silicon's second-order Raman scattering is also observed in the spectrum of PhC slab, as denoted by the green dashed line in Fig. 2(c). In the transmittance spectrum in Fig. 2(b), we can see that the wavelength of this signal (804 nm) also overlaps with the photonic bands, indicating that the double-resonance condition is satisfied for this signal as well. However, in the case of the flat silicon film, this signal was not observed under the same experimental condition, as demonstrated by the blue line in Fig. 2(c). Via the method of double resonance, the submerged signal becomes discernible due to the Raman enhancement provided by the PhC slab.

Further, we measured the spatial distribution of the Raman intensity using Raman spectral mapping techniques. Figure 3(a) shows the

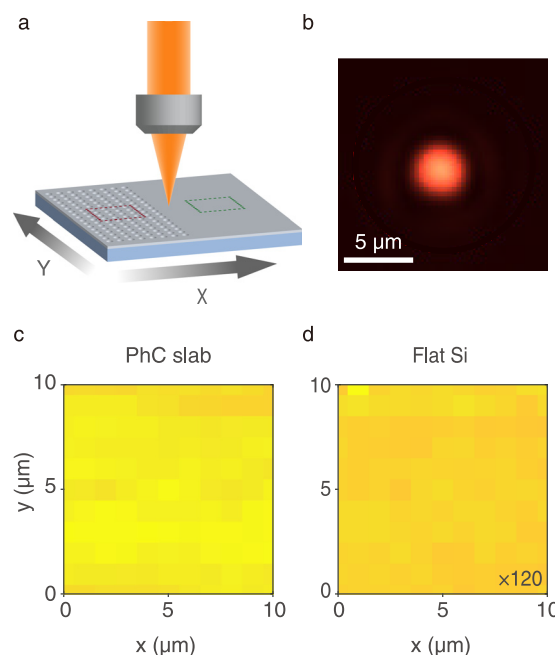


FIG. 3. (a) Schematic of the experimental setup for Raman mapping. (b) The image of the focused laser spot. Scale bar: 5 μm. (c) Raman intensity map for the PhC slab. (d) Raman intensity map for the flat silicon film. The intensities are scaled by 120 times.

schematic of experimental setup for Raman mapping. The laser is focused onto the sample plane through an objective lens (20X, NA = 0.25). Figure 3(b) displays the image of the focused laser spot, which has a size of approximately 4 μm. The sample is moved by a translation stage along X and Y directions to facilitate position scanning across the plane. The step of the position scanning is set as 1 μm. At each position, the Raman spectrum is measured under the excitation of the focused laser spot. Then, the spatial distribution of Raman intensity can be mapped using the intensity of first-order Raman peak in each spectrum. Figure 3(c) shows the Raman intensity map of the PhC slab. For comparison, Fig. 3(d) shows the Raman intensity map measured from an unstructured silicon film region, which is scaled by 120 times. It demonstrates that the Raman enhancement induced by double optical resonances is uniformly distributed due to the periodicity of the PhC slab. This suggests that the PhC slab can serve as a uniform platform for SERS sensing applications.

In addition, we performed experiments to compare the Raman enhancement induced by single-resonance and double-resonance conditions by adjusting the period and hole diameter of the PhC slab. Figures 4(a) and 4(b) show the measured transmittance spectra of these samples. For the sample corresponding to Fig. 4(a), the photonic band overlaps with the frequency of excitation laser (ω). For the sample corresponding to Fig. 4(b), the photonic bands overlap with the frequency of silicon's first-order Raman peak (ω'). The scanning electron microscope (SEM) images of these two samples are shown in the [supplementary material](#), Fig. S5. We measured the Raman spectra for these samples under the same experimental condition as in Fig. 2(c).

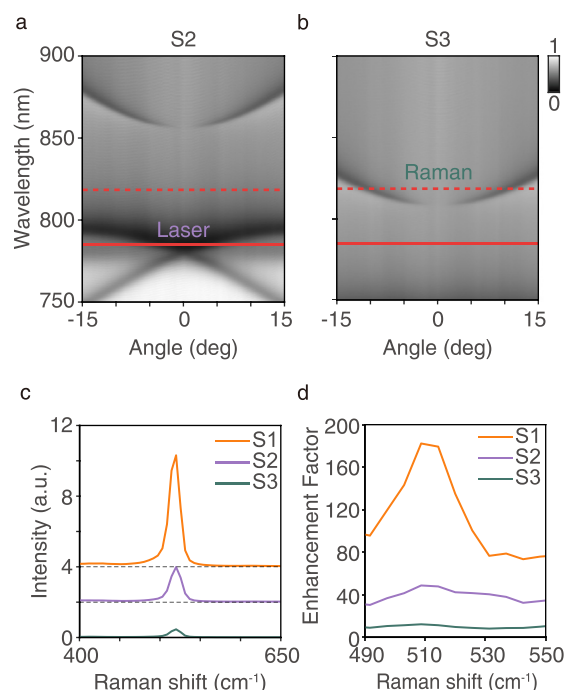


FIG. 4. (a, b) Measured angle-resolved transmittance spectra of the fabricated PhC slabs with single-resonance condition for (a) laser and (b) Raman scattering light. The wavelengths of laser and first-order Raman peak are marked by the solid line and dashed line. (c) Raman spectra of all three samples. S1 and S2 are offset by +4 and +2. S1 corresponds to the sample shown in Fig. 2(b). S2 corresponds to the sample shown in Fig. 4(a), and S3 corresponds to the sample shown in Fig. 4(b). (d) Enhancement factors for all three samples.

Figure 4(c) shows the first-order Raman spectra of all three samples. Spectrum S1 corresponds to the sample with the double-resonance condition shown in Fig. 2(b). Spectra S2 and S3 correspond to the sample with the single-resonance condition shown in Figs. 4(a) and 4(b), respectively. The enhancement factors for each sample are calculated and presented in Fig. 4(d). It shows that the approach of double resonance provides a larger enhancement for Raman signals compared to the single-resonance case. The enhancement factors that take into account the area ratio of silicon for each sample are also shown in the [supplementary material](#), Fig S6. It shows that the sample with the double-resonance condition still presents a larger enhancement factor than the other two samples using this calculation method.

In conclusion, we have designed and fabricated a PhC slab that satisfies double-resonance conditions to enhance the Raman signals of silicon. The enhancement is uniformly distributed across the PhC slab. Compared with single-resonance cases, the double-resonance approach achieves a larger enhancement factor for the Raman signal. It provides a perspective for the design of all-dielectric SERS substrates and may have potential applications in chemical sensing, biological analysis, and medical diagnostics.

See the [supplementary material](#) for the information including (1) the experimental setup for angle-resolved transmittance spectra and Raman spectra, (2) the experimental results for the line shape deviation

of Raman peak under double-resonance enhancement, (3) the experimental results for the response of enhanced Raman intensity to the power of excitation laser, (4) the SEM images of samples S2 and S3, and (5) the enhancement factor that take into account the effective enhancement area for all three samples.

This work is supported by the National Natural Science Foundation of China (Nos. T2394480, T2394481, 12221004, 12234007, and 12321161645); the National Key R&D Program of China (Nos. 2022YFA1404800 and 2023YFA1406900); and the Science and Technology Commission of Shanghai Municipality (Nos. 22142200400, 21DZ1101500, 2019SHZDZX01, and 23DZ2260100). J. W. is further supported by China National Postdoctoral Program for Innovative Talents (BX20230079) and China Postdoctoral Science Foundation (No. 2023M740721).

AUTHOR DECLARATIONS

Conflict of Interest

The authors have no conflicts to disclose.

Author Contributions

Yuyang Xu: Conceptualization (equal); Data curation (equal); Investigation (equal); Writing – original draft (lead); Writing – review & editing (equal). **Shunben Wu:** Conceptualization (equal); Data curation (equal); Investigation (equal); Writing – review & editing (equal). **Shaolin Hong:** Conceptualization (equal); Investigation (equal); Writing – review & editing (equal). **Xinhao Wang:** Data curation (equal); Investigation (equal); Writing – review & editing (equal). **Xiaohan Liu:** Investigation (equal); Resources (equal). **Jiajun Wang:** Conceptualization (equal); Investigation (equal); Resources (equal); Writing – review & editing (equal). **Lei Shi:** Conceptualization (equal); Investigation (equal); Resources (equal); Writing – review & editing (equal).

DATA AVAILABILITY

The data that support the findings of this study are available from the corresponding authors upon reasonable request.

REFERENCES

- ¹A. Campion and P. Kambhampati, “Surface-enhanced Raman scattering,” *Chem. Soc. Rev.* **27**, 241–250 (1998).
- ²K. Kneipp, “Surface-enhanced Raman scattering,” *Phys. Today* **60**(11), 40–46 (2007).
- ³X. Cong, X.-L. Liu, M.-L. Lin, and P.-H. Tan, “Application of Raman spectroscopy to probe fundamental properties of two-dimensional materials,” *npj 2D Mater. Appl.* **4**, 13 (2020).
- ⁴X. Zhang, X.-F. Qiao, W. Shi, J.-B. Wu, D.-S. Jiang, and P.-H. Tan, “Phonon and Raman scattering of two-dimensional transition metal dichalcogenides from monolayer, multilayer to bulk material,” *Chem. Soc. Rev.* **44**, 2757–2785 (2015).
- ⁵M. Arabi, A. Ostovan, Y. Wang, R. Mei, L. Fu, J. Li, X. Wang, and L. Chen, “Chiral molecular imprinting-based SERS detection strategy for absolute enantiomeric discrimination,” *Nat. Commun.* **13**, 5757 (2022).
- ⁶J. E. Park, N. Yonet-Tanyeri, E. Vander Ende, A.-I. Henry, B. E. Perez White, M. Mrksich, and R. P. Van Duyne, “Plasmonic microneedle arrays for in situ sensing with surface-enhanced Raman spectroscopy (SERS),” *Nano Lett.* **19**, 6862–6868 (2019).

- ⁷J.-H. Choi, T.-H. Kim, W. A. El-Said, J.-H. Lee, L. Yang, B. Conley, J.-W. Choi, and K.-B. Lee, "In situ detection of neurotransmitters from stem cell-derived neural interface at the single-cell level via graphene-hybrid SERS nanobiosensing," *Nano Lett.* **20**, 7670–7679 (2020).
- ⁸F. Sun, H.-C. Hung, A. Sinclair, P. Zhang, T. Bai, D. D. Galvan, P. Jain, B. Li, S. Jiang, and Q. Yu, "Hierarchical zwitterionic modification of a SERS substrate enables real-time drug monitoring in blood plasma," *Nat. Commun.* **7**, 13437 (2016).
- ⁹R. Haldavnekar, K. Venkatakrishnan, and B. Tan, "Non plasmonic semiconductor quantum SERS probe as a pathway for in vitro cancer detection," *Nat. Commun.* **9**, 3065 (2018).
- ¹⁰J. U. Lee, W. H. Kim, H. S. Lee, K. H. Park, and S. J. Sim, "Quantitative and specific detection of exosomal mirnas for accurate diagnosis of breast cancer using a surface-enhanced Raman scattering sensor based on plasmonic head-flocked gold nanopillars," *Small* **15**, 1804968 (2019).
- ¹¹K. Kong, C. Kendall, N. Stone, and I. Notingher, "Raman spectroscopy for medical diagnostics—from in-vitro biofluid assays to in-vivo cancer detection," *Adv. Drug Delivery Rev.* **89**, 121–134 (2015).
- ¹²Y. Yu, T.-H. Xiao, Y. Wu, W. Li, Q.-G. Zeng, L. Long, and Z.-Y. Li, "Roadmap for single-molecule surface-enhanced Raman spectroscopy," *Adv. Photonics* **2**, 014002 (2020).
- ¹³B. Sharma, R. R. Frontiera, A.-I. Henry, E. Ringe, and R. P. Van Duyne, "SERS: Materials, applications, and the future," *Mater. Today* **15**, 16–25 (2012).
- ¹⁴I. Alessandri and J. R. Lombardi, "Enhanced Raman scattering with dielectrics," *Chem. Rev.* **116**, 14921–14981 (2016).
- ¹⁵R. Pilot, R. Signorini, C. Durante, L. Orian, M. Bhamidipati, and L. Fabris, "A review on surface-enhanced Raman scattering," *Biosensors* **9**, 57 (2019).
- ¹⁶J. R. Lombardi and R. L. Birke, "A unified view of surface-enhanced Raman scattering," *Acc. Chem. Res.* **42**, 734–742 (2009).
- ¹⁷M. G. Albrecht and J. A. Creighton, "Anomalously intense Raman spectra of pyridine at a silver electrode," *J. Am. Chem. Soc.* **99**, 5215–5217 (1977).
- ¹⁸P. Karthick Kannan, P. Shankar, C. Blackman, and C.-H. Chung, "Recent advances in 2D inorganic nanomaterials for SERS sensing," *Adv. Mater.* **31**, 1803432 (2019).
- ¹⁹C. Liang, Z.-A. Lu, M. Zheng, M. Chen, Y. Zhang, B. Zhang, J. Zhang, and P. Xu, "Band structure engineering within two-dimensional borocarbonitride nanosheets for surface-enhanced Raman scattering," *Nano Lett.* **22**, 6590–6598 (2022).
- ²⁰G. Demirel, R. L. Gieseck, R. Ozdemir, S. Kahmann, M. A. Loi, G. C. Schatz, A. Facchetti, and H. Usta, "Molecular engineering of organic semiconductors enables noble metal-comparable SERS enhancement and sensitivity," *Nat. Commun.* **10**, 5502 (2019).
- ²¹Y. Chen, Z.-H. Zhou, C.-L. Zou, Z. Shen, G.-C. Guo, and C.-H. Dong, "Tunable Raman laser in a hollow bottle-like microresonator," *Opt. Express* **25**, 16879–16887 (2017).
- ²²R.-S. Liu, W.-L. Jin, X.-C. Yu, Y.-C. Liu, and Y.-F. Xiao, "Enhanced Raman scattering of single nanoparticles in a high-Q whispering-gallery microresonator," *Phys. Rev. A* **91**, 043836 (2015).
- ²³I. Shlesinger, K. G. Cognée, E. Verhagen, and A. F. Koenderink, "Integrated molecular optomechanics with hybrid dielectric-metallic resonators," *ACS Photonics* **8**, 3506–3516 (2021).
- ²⁴Y.-F. Xiao, C.-L. Zou, Y. Li, C.-H. Dong, Z.-F. Han, and Q. Gong, "Asymmetric resonant cavities and their applications in optics and photonics: A review," *Front. Optoelectron. China* **3**, 109–124 (2010).
- ²⁵S.-J. Tang, M. Zhang, J. Sun, J.-W. Meng, X. Xiong, Q. Gong, D. Jin, Q.-F. Yang, and Y.-F. Xiao, "Single-particle photoacoustic vibrational spectroscopy using optical microresonators," *Nat. Photonics* **17**, 951–956 (2023).
- ²⁶W. Gomulya, H. Machiya, K. Kashiwa, T. Inoue, S. Chiashi, S. Maruyama, and Y. K. Kato, "Enhanced Raman scattering of graphene using double resonance in silicon photonic crystal nanocavities," *Appl. Phys. Lett.* **113**, 081101 (2018).
- ²⁷S. G. Johnson, S. Fan, P. R. Villeneuve, J. D. Joannopoulos, and L. Kolodziejski, "Guided modes in photonic crystal slabs," *Phys. Rev. B* **60**, 5751 (1999).
- ²⁸S. Fan and J. D. Joannopoulos, "Analysis of guided resonances in photonic crystal slabs," *Phys. Rev. B* **65**, 235112 (2002).
- ²⁹Y. Chang, D. Hasan, B. Dong, J. Wei, Y. Ma, G. Zhou, K. W. Ang, and C. Lee, "All-dielectric surface-enhanced infrared absorption-based gas sensor using guided resonance," *ACS Appl. Mater. Interfaces* **10**, 38272–38279 (2018).
- ³⁰N. Bernhardt, K. Koshelev, S. J. White, K. W. C. Meng, J. E. Froch, S. Kim, T. T. Tran, D.-Y. Choi, Y. Kivshar, and A. S. Solntsev, "Quasi-BIC resonant enhancement of second-harmonic generation in WS₂ monolayers," *Nano Lett.* **20**, 5309–5314 (2020).
- ³¹S. Romano, G. Zito, S. Managò, G. Calafiore, E. Penzo, S. Cabrini, A. C. De Luca, and V. Mocella, "Surface-enhanced Raman and fluorescence spectroscopy with an all-dielectric metasurface," *J. Phys. Chem. C* **122**, 19738–19745 (2018).
- ³²H. Hu, A. K. Pal, A. Berestennikov, T. Weber, A. Stefancu, E. Cortés, S. A. Maier, and A. Tittl, "Surface-enhanced Raman scattering in BIC-driven semiconductor metasurfaces," *Adv. Opt. Mater.* **12**, 2302812 (2024).
- ³³W. Mao, Y. Li, X. Jiang, Z. Liu, and L. Yang, "A whispering-gallery scanning microprobe for Raman spectroscopy and imaging," *Light Sci. Appl.* **12**, 247 (2023).
- ³⁴Y. Zhang, A. Chen, W. Liu, C. W. Hsu, B. Wang, F. Guan, X. Liu, L. Shi, L. Lu, and J. Zi, "Observation of polarization vortices in momentum space," *Phys. Rev. Lett.* **120**, 186103 (2018).
- ³⁵Y. Zhang, M. Zhao, J. Wang, W. Liu, B. Wang, S. Hu, G. Lu, A. Chen, J. Cui, W. Zhang *et al.*, "Momentum-space imaging spectroscopy for the study of nanophotonic materials," *Sci. Bull.* **66**, 824–838 (2021).
- ³⁶E. C. Le Ru and B. Auguié, "Enhancement factors: A central concept during 50 years of surface-enhanced Raman spectroscopy," *ACS nano* **18**, 9773–9783 (2024).